

# PETRIC - A Positron Emission Tomography Readout Integrated Circuit

M. Pedrali-Noy, *Member, IEEE*, G. Gruber, B. Krieger, *Member, IEEE*, E. Mandelli, *Member, IEEE*, G. Meddeler, *Member, IEEE*, W. Moses, *Senior Member, IEEE*, and V. Rosso

**Abstract**— We present architecture, critical design issues and performance measurements of PETRIC, a 64-channel mixed signal front-end integrated circuit (IC) for reading out a photodiode (PD) array coupled with LSO scintillator crystals for a medical imaging application (PET). Each channel consists of a low noise charge sensitive pre-amplifier (CSA), a RC-CR pulse shaper and a winner-take-all (WTA) multiplexer that selects the channel with the largest input signal. Triggered by an external timing signal, a switch opens and a capacitor stores the peak voltage of the winner channel. The shaper rise and fall times are adjustable by means of external current inputs over a continuous range of 0.7  $\mu\text{s}$  to 9  $\mu\text{s}$ . Power consumption is 5.4 mW per channel, measured Equivalent Noise Charge (ENC) at 1  $\mu\text{s}$  peaking time, zero leakage current is 33 rms electrons plus 7.3 rms electrons per pF of input capacitance. Design is fabricated in 0.5  $\mu\text{m}$  3.3V CMOS technology.

## I. INTRODUCTION

WE are designing a Positron Emission Tomography (PET) detector module to identify 511 keV photons generated by positron annihilation with good spatial and temporal resolution. The detector module consists of a 8 x 8 cerium-doped lutetium oxyorthosilicate ( $\text{Lu}_2\text{SiO}_5[\text{Ce}]$  or LSO) scintillator crystal array coupled on one side to a 8 x 8 photodiode (PD) array of 3  $\text{mm}^2$  pixels, on the other to a single channel Photomultiplier Tube (PMT). Whenever a gamma ray interacts in the scintillator array, a timing and an energy signal are generated by the PMT, and an energy signal is generated in the PD array. The PMT provides an accurate timing pulse and initial energy discrimination for the 64 crystals in the module while the PD array identifies the crystal of interaction. The sum of the charges collected at the PMT end and at the PD end, PD+PMT, provides a total energy signal while the depth estimator ratio  $\text{PD}/(\text{PD}+\text{PMT})$

determines the Depth Of Interaction (DOI) in the crystal. Fig. 1 shows the detector module.

The large number of electrons generated by the LSO crystal during gamma interaction (3000 to 5000) makes the noise due to statistical fluctuation in photon emission in the PMT negligible. The electronic noise at the PD end is important, given the constraints of the detector capacitance ( $\sim 3\text{pF}$ ), leakage current (300 pA) and data rate (peaking time  $\sim 1\mu\text{s}$ ) and thus must be minimized [1]. The identification of the crystal of interaction has to occur in a short time compared to the expected period between different input events (10  $\mu\text{s}$ /detector module).

PETRIC provides a unique mixed-signal solution to readout the signal from PD array through the novel on-chip integration of an array of highly sensitive amplifier channels with a Winner-Take-All multiplexer.

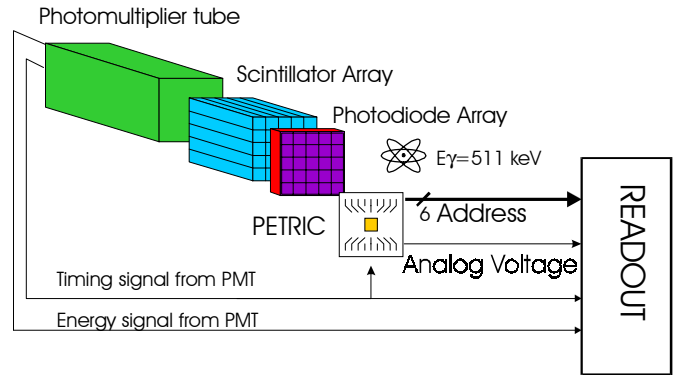


Fig. 1. Elements of the PET Camera Detector Module. The IC sits on a printed circuit board used to fan-in the PD array. The IC continuously amplifies the energy signals from the PD array and produces at its output an analog pulse whose peak amplitude is proportional to the charge collected in the channel with the largest input signal (winner channel) and the 6-bit digital address of the winner channel. The timing signal from the PMT can be used to Track-and-Hold the output analog pulse.

## II. INTEGRATED CIRCUIT REQUIREMENTS AND IMPLEMENTATION

The use of CMOS amplifiers for PET front-end electronics was evaluated in [2]. Our IC has to simultaneously acquire input signals and perform analog and digital readout; it can be set in the desired configuration (gain, channel masking) before acquisition and readout begin. Input signals come from a 64 pixel photodiode array DC coupled to the IC; each

Manuscript received Nov 5, 2000. This work was supported in part by the U.S. Department of Energy under Contract No. DE-AC03-76SF00098, and in part by Public Health Service Grant Nos. P01-HL25840 and R01-CA67911.

M. Pedrali-Noy is with the Lawrence Berkeley National Laboratory, Integrated System Group, Berkeley CA, USA 94709 (e-mail: [mpedrali-noy@lbl.gov](mailto:mpedrali-noy@lbl.gov)).

G. Gruber, B. Krieger, E. Mandelli, G. Meddeler, W. Moses are with the Lawrence Berkeley National Laboratory.

V. Rosso is with the Dipartimento di Fisica dell'Universita' e sezione INFN, San Piero a Grado, Pisa, Italy 56010

photodiode has a shunt capacitance  $C_d$  of  $\sim 3$  pF and a dark leakage current  $I_{\text{dark}}$  in the range of 100 to 600 pA. The IC continuously outputs the amplified pulse signal corresponding to the element of the array with the highest signal and its digital address. The peaking time and the gain must be adjustable to comply with different signal/data-rate systems. An externally generated Track-and-Hold signal stores the pulse peak voltage on an on-chip capacitor. Electronic noise should dominate; therefore it must be minimized. To achieve a reasonable Signal-to-Noise ratio the total input referred noise should be less than 200 electrons rms. Noise contributions from the electronic readout and from the leakage current of the detector have been studied extensively in the field of electronics for high-energy physic experiments [3]. Power consumption should be minimized since the module that hosts the IC does not provide cooling. We have selected a  $0.5 \mu\text{m}$  3.3 V CMOS technology with silicide block and linear capacitor options based on current availability. We have fabricated and tested a 16-channel amplifier prototype and a 16-channel WTA prototype; these prototype designs, with minimal modification, were merged and expanded to realize the 64 channel IC. Noise coefficients for  $1/f$  noise extracted from prototype measurement showed that the  $1/f$  noise contribution to the Equivalent Noise Charge (ENC) is relevant at our target shaping time and input leakage current.

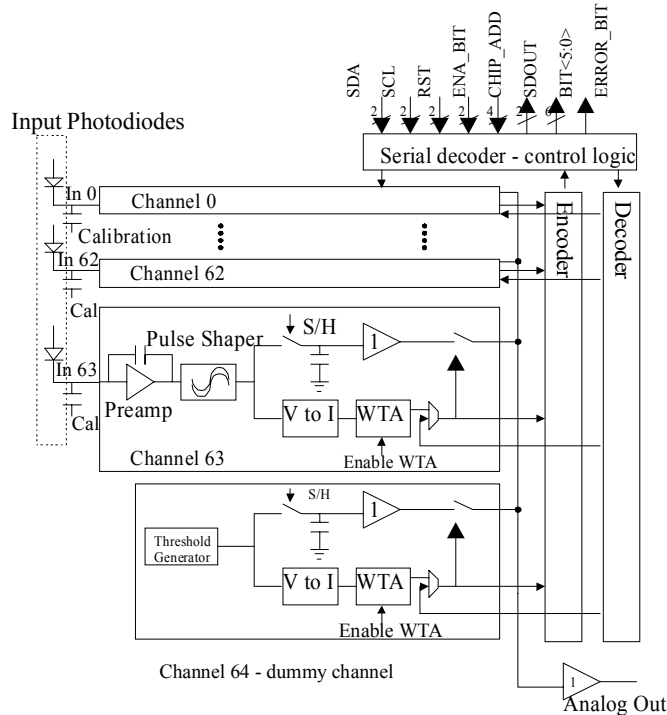


Fig. 2. PETRIC Architecture. Each channel consists of a pulse amplifier (CSA and RC-CR filter) and a WTA cell. When a WTA cell recognizes its amplifier channel as producing the largest output voltage a hit bit is generated. This bit is encoded to produce the address of the winner channel.

The chip architecture is shown in Fig. 2. Input charge signals are pre-amplified and filtered to optimize signal to noise ratio. The Winner-Take-All (WTA) circuit, DC coupled to the amplifier outputs, continuously selects the channel with the largest input and connects it to an output buffer.

A dummy channel, without an amplifier, presents a DC only voltage to the WTA and acts like a threshold that the other channels need to exceed in order to be identified as the winner. The dummy channel should be selected when no input signal comes from the PD array and prevents the WTA from switching due to electronic noise. The choice of the threshold voltage comes from consideration of several factors: the random electronic noise at the output of the amplifier channel, the noise coupling from the switching circuit to the sensitive amplifiers, the DC output dispersion of the amplifiers and the DC input dispersion of the WTA. The threshold should be large enough to prevent switching due to noise, while it should be small enough to allow identification of small signals.

Triggered by an off-chip signal, a Track-and-Hold capacitor can store the analog peak voltage. The control logic sets the preamplifiers' gains, masks individual channels from the WTA and connects a calibration circuit for testing. For minimum cross talk between the digital and the sensitive analog sections it is possible to gate the digital signal from the WTA to the encoder: in this way the encoder can be activated after the peak voltage has been stored in the holding capacitor.

### III. CIRCUIT DESIGN AND LAYOUT

#### A. Amplifier Channel

The amplifier channel consists of a low-noise charge sensitive amplifier (CSA) followed by a RC-CR shaper and AC amplifier.

##### 1) Charge Sensitive Preamplifier

The single-ended CSA consists of a common source cascode stage with regulated cascodes to boost DC gain, followed by a source follower stage. A simplified schematic is shown in Fig. 3. The input device  $M_{\text{inp}}$  is a PMOS with gate capacitance  $C_{\text{inp}}$ ; the size of  $M_{\text{inp}}$  has been chosen as a compromise between  $1/f$  noise minimization ( $C_{\text{inp}} = C_d$ ) and thermal noise minimization ( $C_{\text{inp}} = 1/3 C_d$ ) [4]. The bias current of  $M_{\text{inp}}$ , given by  $I_{\text{inp}} = I1+I2$ , sets  $M_{\text{inp}}$  in the region of operation at the onset of strong inversion to obtain a reasonable  $g_m/I_{\text{inp}}$  ratio while achieving a high transconductance  $g_m \sim 8\text{mS}$  [5]. The main noise contribution to the noise of the CSA comes from  $M_{\text{inp}}$ , although the noise contribution from the current sources  $I1$  and  $I2$  are not negligible due to the low power supply and the limited voltage available to degenerate them [6]. The feedback capacitance  $C_f$  is placed between the input node IN and the gate of the source follower stage to avoid introduction on the closed loop of the complex poles of the follower stage and to isolate the feedback capacitor from the following stage. Switching between different feedback capacitors allows different gains to be achieved. The low-level input signal requires a small feedback capacitance to achieve a reasonable gain at the preamplifier output. With a choice of  $C_f = 14$  fF for the maximum gain setting in the preamplifier, the feedback factor  $f$ , given by

$$f = \frac{C_f}{C_d + C_{inp} + C_{parasitic}} \quad (1)$$

is  $f = 2.3 \times 10^{-3}$ . This small feedback factor provides high gain and relaxes the design constraints for closed loop stability, at the expense of a slower response of the preamplifier. Charge restoring is provided by minimum length PMOS reset transistor  $M_f$  ( $W/L = 2.4/0.6 \mu\text{m}$ ) that is biased to operate in the saturation region.  $M_f$  adds negligible parasitic capacitance to the feedback capacitance, although its minimum size could result in a spread of its output resistance due to mismatch and thus channel-to-channel reset time variations. Achieved Drain to Source resistance  $R_{ds}$  is 14 to 3  $\text{G}\Omega$  in the 100 to 500 pA range; at zero leakage current the maximum achievable  $R_{ds}$  is limited by the MOS source and drain diode leakage current to 70  $\text{G}\Omega$ . The DC biasing of  $M_f$  is provided by a replica bias like in [7]. Due to the direction of the leakage current  $M_f$  operates at constant gate-to-source voltage; a large spread in the leakage current dictates adjustment of the bias on a channel-by-channel basis. This is accomplished by an on-chip DAC.

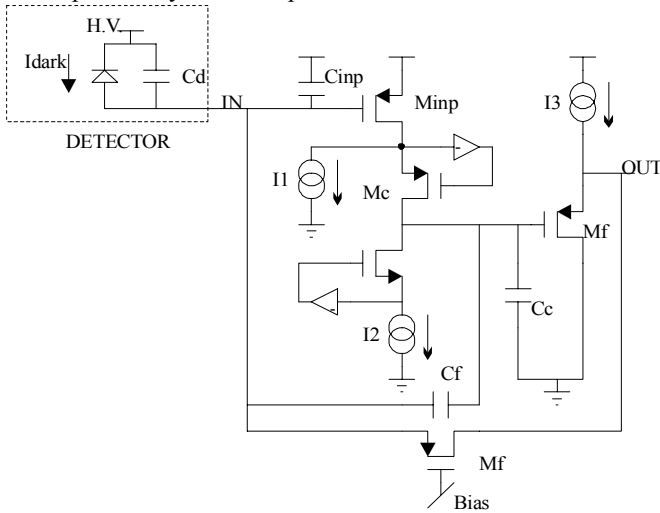


Fig. 3. Simplified schematic of the CSA. The telescopic cascode design still fits in 3V power supply but will require folding for lower voltage operation.

## 2) Pulse Shaper

The pulse shaper is a two stage Gm-C filter and it is a single-ended, first order version of the design presented in [8]. A simplified schematic is shown in Fig. 4. The two identical Operational Transconductance Amplifiers (OTAs) OTA1 and OTA2 that determine the time constants are based on the design presented in [9]; they use transistors operated in the triode region to degenerate their input differential pairs. The OTAs' tail current can be externally adjusted to modify their transconductance and achieve the desired shaping time. The filter is followed by an AC amplifier that provides no shaping, due to the long time constant introduced by OTA3 and its feedback capacitance; this block eases the requirements of large signal linearity of the preceding blocks at the expense of power consumption.

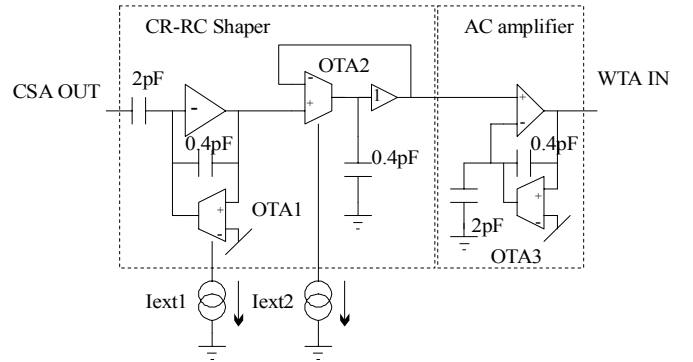


Fig. 4. Simplified schematic of the pulse shaper. Two external currents  $I_{ext1}$  and  $I_{ext2}$  are used to tune the transconductances of the OTAs and thus to change the pulse shaping time.

## B. Winner-Take-All

The Winner-Take-All (WTA) circuit is DC coupled to the previous amplifier stage and is based on the design presented in [10]; it consists of a Voltage-to-Current (VtoI) converter followed by a high gain non-linear differential circuit. A simplified schematic is shown in Fig. 5. The VtoI circuit consists of a resistor followed by a common gate stage. The WTA cells in each channel share a common tail current  $I_{com}$  that is taken by the channel with the largest input, like in a large-signal driven differential pair. The channel with the highest input voltage has  $I_{out} = I_{com}$  while all the others  $I_{out}$  is  $\sim 0$ ; a current comparator compares the output current of each channel to a fixed current and generates the logic signal that identifies the winning channel. Due to its high gain, the main source of error of the WTA is due to mismatch of the transistors and resistors in the VtoI. The selection circuit is designed to have a first-order response and a GBW product of 8 MHz.

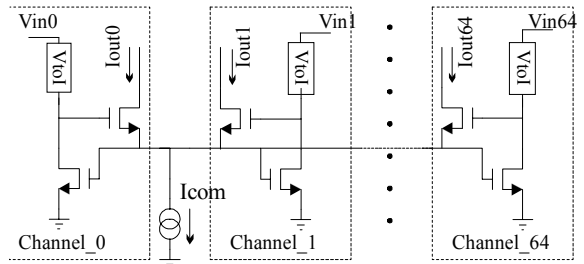


Fig. 5. Simplified schematic of the WTA. Based on a two-transistor per cell design this circuit is compact and dissipates very little power.  $I_{com}$  is set equal to 15  $\mu\text{A}$  by an external reference.

A DC level shifter sets the DC output voltage of the dummy channel  $\sim 40$  mV above the other channels.

When a switch is toggled by an external signal, the Track and Hold capacitor stores the analog voltage from the preceding stage; charge injection and clock feedthrough are minimized by a compensation scheme [11].

## C. Control Logic

The digital control section has been synthesized from a state-machine diagram using standard cells. The logic uses static, fully synchronous CMOS registers. Decoding a digital

protocol based on the Xicor I2C, this logic circuit controls the gain and reset time constant of the preamplifiers, masks out unwanted channels from the WTA, connects different channels to the calibration capacitance, and produces an error bit when multiple channels are selected. The IC can be set to operate in two different modes: in WTA (default) mode the WTA selects the channel with the highest output signal. In MUX (test) mode the WTA is disabled and a channel selected by the user is connected to the analog output.

#### D. Layout

Fig. 6 shows a microphotograph of the realized circuit. To minimize coupling to the sensitive amplifier from the switching circuitry, separate quiet power supply lines and pads have been utilized for the input transistors' supply, the input transistors' well and the amplifier channel; the WTA, the encoder and the digital section share the same supplies. Non-power carrying substrate contact lines are employed; furthermore to take advantage of the low resistive substrate and to reduce substrate noise coupling the chip back has been gold plated [12]. The layout is pad-limited: the bond pad size and spacing have been dictated by minimum line pitch and bonding constraints on the fan-in printed circuit board that will host the IC. The die area is 4.5 mm x 4.8 mm. The capacitors in the preamplifiers are realized as Metal 1 to Metal 2 plates while all the other capacitors are implemented using the linear capacitor option, i.e. polysilicon-thin\_oxide-p+diffusion. Test pads have been provided at the output of the CSAs, shapers, and AC amplifiers and to monitor the status of the internal digital logic.

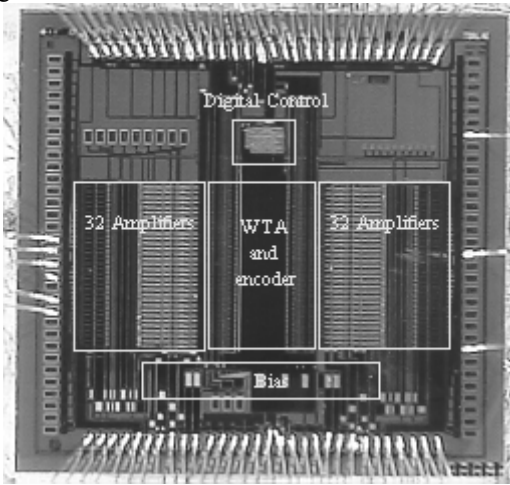


Fig. 6. Microphotograph of the realized IC. The 64 channels are split in two columns and they share a common bias; the WTA cells sit in the center, the digital control logic is on top.

## IV. PERFORMANCE MEASUREMENTS

### A. Amplifier Channel

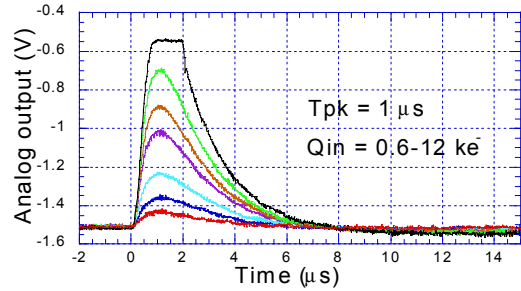


Fig. 7. Voltage output response of a single amplifier channel to different input charges.

#### 1) Gain

We measured the gain of the amplifier's channel using external injection capacitors. Fig. 7 shows the waveforms present at the analog output when different charges are injected into one amplifier. At maximum gain setting ( $120\text{mV}/1000e^-$ ),  $1\mu\text{s}$  peaking time (achieved with equal RC and CR time constants in the shaper), detector capacitance  $C_d = 3.7\text{ pF}$ , the gain is linear within 1% in the range of 750 to 4000 electrons input charge. For higher input charges ( $5ke^-$  to  $9ke^-$ ) the non-linearity of the pulse shaper degrades the performance and finally the output stage enters into saturation for input charges bigger than  $9ke^-$ .

Using the internal calibration circuit we have measured 3% relative rms gain dispersion between channels on the same IC.

#### 2) Pulse Shaping

Adjusting the external currents shaping times are achievable in the range of 0.7 to  $9\mu\text{s}$  as shown in Fig. 8.

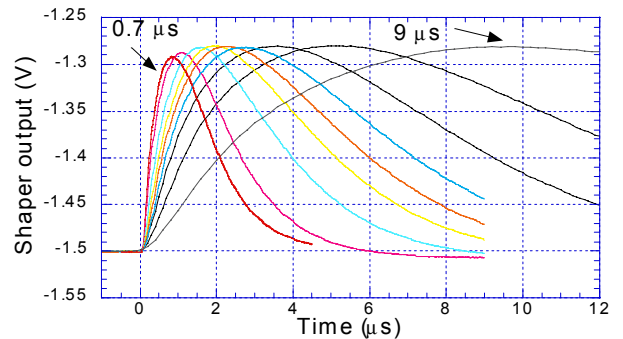


Fig. 8. Voltage output response of a single channel to an 1800 electrons input charge for different values of the external current sources of the shaper stage.

#### 3) DC Output Offset Voltage

The DC dispersion at the output of the amplifier channel is determined by the input random offset of the feedback transistor of the AC amplifier. Measurements show a value for the DC offset variation of 8 mV rms.

#### 4) Electronic Noise

Noise measurements were performed on a test board, since a detector module was not yet available at the time of publication of this paper. The characterization of the chip noise performances was carried out on both unbonded

channels (no external load) and on channels that were bonded to outside loading capacitors. Input ENC was measured on each channel as the standard deviation of the output peak voltage distribution, assumed to be gaussian. In Fig. 9 the results of the measurements are plotted as a function of the input external capacitance at a filter peaking time setting of 1 $\mu$ s. Even if these data do not take into account any leakage detector current, the results confirm noise performances well below the required 200 electrons specification for a foreseen 3pF load. Noise performances were also measured as a function of the filter peaking time setting, as plotted in Fig. 10, to extrapolate the 1/f noise floor limit, for three different input capacitances. The data in this plot report a dominance of white noise contribution until 10 $\mu$ s peaking time and confirm an ENC scaling with capacitance equal to 7.2 electrons per pF. As a crosscheck, input referred noise spectral density was extracted from measurements and compared to the expected one. In a linear system the input referred noise charge can be expressed as

$$ENC^2 = S_w \frac{A_1}{\tau} C_{TOT}^2 + A_2 C_{TOT}^2 S_{1/f} + A_3 \tau S_{||} \quad (2)$$

where  $S_w$  is the input noise spectral density,  $A_1$  is the white series noise coefficient,  $A_2$  is the 1/f series noise coefficient,  $A_3$  is the parallel noise coefficient,  $C_{TOT}$  is the total input capacitance and  $\tau$  is the filter peaking time [13]. At 1 $\mu$ s peaking time, the filter bandwidth is large enough to assume that the white noise contribution to the total input noise is dominant, in absence of parallel noise. The relation between ENC and input capacitance is linear and the input white noise spectrum can be inferred from the measurements.

$$S_w = \frac{\tau}{A_1} \left[ \frac{\partial ENC}{\partial C_D} \right]^2 \quad (3)$$

With a measured  $A_1$  value close to 1, the preamplifier input white noise spectral density is 1.3 nV/ $\sqrt$ Hz in agreement with the simulation results. Data in Fig. 10 confirm the result, with and extracted 1.4 nV/ $\sqrt$ z against an input device simulated noise of 1.2 nV/ $\sqrt$ Hz.

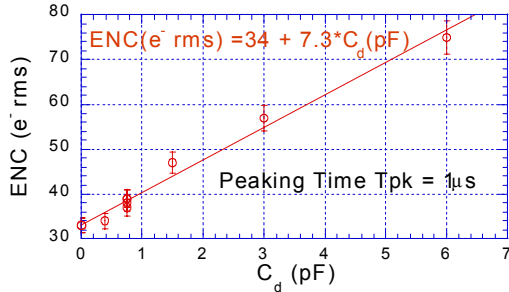


Fig. 9. ENC vs. peaking time for different detector capacitances.

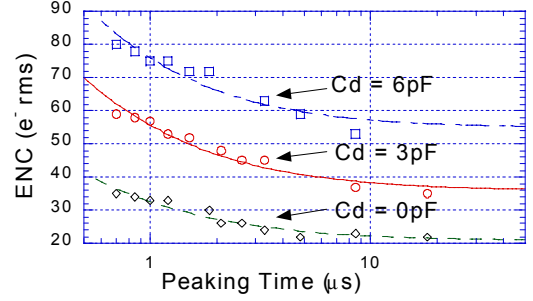


Fig. 10. ENC vs. detector capacitance  $C_d$  at 1  $\mu$ s peaking time. Data are fitted neglecting the parallel noise contribution.

## B. Amplifiers and Winner-Take-All

### 1) Channel Selection

The WTA selects the input channel with the highest dc voltage in less than 150 ns, connects it to the analog buffer amplifier, and outputs the digital address bits of the winning channel. In Fig. 11 two recognizable RC-CR shaped pulse are shown at the analog output of the IC. The time that the WTA takes to identify the winner channel is the sum of the switching times of the WTA cell, the current comparator and the decoder.

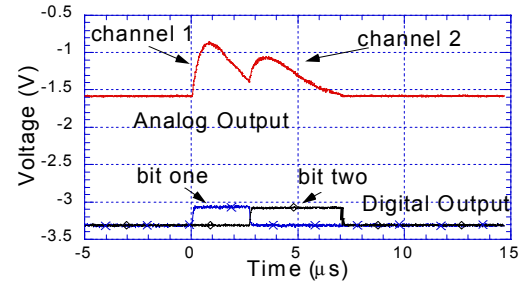


Fig. 11. Two different input signal charges are injected in two different channels. The first signal  $Q_1$  is injected at time zero while the second signal  $Q_2$  ( $Q_1 > Q_2$ ) is injected after  $\sim 2.5 \mu$ s. The analog output tracks the pulse generated by  $Q_1$  until the pulse generated by  $Q_2$  becomes higher in voltage. The digital output bits toggle accordingly.

### 2) Input DC Threshold Dispersion

Connecting two channels at the time to the WTA, one channel with no input signal and the dummy threshold channel, we have varied the threshold channel voltage until the other channel would be identified as the winner. We have measured 20 mV rms DC dispersion at the input of the WTA. This value is the sum of the output dispersion of the amplifier channel and of the input dispersion of the WTA channel. Since the measured DC output dispersion of the amplifiers is 8 mV rms it is the WTA circuit input dispersion that dominates. When no input signal is present at the amplifier inputs, the dummy channel is always selected as the winner by the WTA.

### 3) Track-and-Hold

The output analog voltage of the amplifier channel is stored in a 400fF holding capacitor when the hold signal is received by the IC. Track-and-Hold operation is shown in Fig. 12. The measured voltage error in the holding capacitor due to clock

feedthrough and charge injection is less than 4 mV; the error is signal dependent and could be minimized increasing the holding capacitor size from its current value, at the expense of loading the previous stage.

The performances of the IC are summarized in Table I.

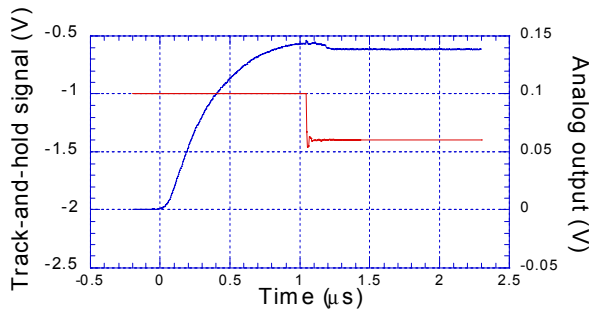


Fig. 12. The analog voltage is stored in the holding capacitor when the Track-and-Hold signal toggles.

TABLE I  
SUMMARY OF THE IC'S PERFORMANCES

Technology	CMOS 0.5 $\mu\text{m}$ 3.3 V
Die Area	4.5 mm x 4.8 mm
Leakage Current	30 – 600 pA
Detector Capacitance	3 pF
Number of Channels	64
Max Gain	120mV/1000e <sup>-</sup>
Min Gain	40 mV/1000e <sup>-</sup>
Shaping	0.7 to 9 $\mu\text{s}$ unipolar
Noise at 1 $\mu\text{s}$ Tpk	34 + 7.2*Cd(pF) e <sup>-</sup> rms
Power	5.4 mW/Channel

## V. CONCLUSIONS

Compactness, high performances and flexibility make PETRIC a unique and ideal solution for PET camera modules front-end readout. Due to the flexibility of its architecture and of the analog front end, the IC is well suited for any application employing low capacitance PD detectors in moderate to high data rate environments and it is currently considered for single photon cameras readout [14].

Future directions of this work include on-chip integration of a peak detection circuit and band-gap voltage reference, a self-adjusting reset scheme in the preamplifier and a characterization of the Electro Static Discharge (ESD) protection structures for production development.

## VI. ACKNOWLEDGMENT

We thank Prof. P.F. Manfredi for the fruitful discussions, and acknowledge the valuable help of M. Ho for designing the test boards and the detector module, and G. Zizka for bonding several ICs. This work was supported in part by the Director, Office of Energy Research, Office of Health and Environmental Research, Medical Applications and Biophysical Research Division of the U.S. Department of Energy under contract No. DE-AC03-76SF00098, in part by the National Institutes of Health, National Heart, Lung, and

Blood Institute, National Cancer Institute under grants No. P01-HL25840 and No. R01-CA67911. This research was supported by the Laboratory Technology Research Division SC-32, (formerly called ER LTT), Office of Science, US Department of Energy under a CRADA (Cooperative Research and Development Agreement) between Lawrence Berkeley National Laboratory and Capintec, Inc., Ramsey, NJ under US DOE Contract DE-AC03-76SF00098.

## VII. REFERENCES

- [1] J. Huber, W. Moses, M. Andreaco, and O. Petterson, "A LSO scintillator array for a PET detector module with depth of interaction measurement," *IEEE Trans. Nucl. Sci.*, (Submitted for Publication).
- [2] W. Moses, I. Kipnis, and M. Ho, "A 16-channel charge sensitive amplifier IC for a PIN photodiode array based PET detector module," *IEEE Trans. Nucl. Sci.*, vol. 41, pp. 1469–1472, 1994.
- [3] E. Gatti, P. Manfredi, "Processing the signals from solid-state detectors in elementary particle physics," *Nuovo Cimento*, 1986 vol 9 no. 1.
- [4] Z. Chang, W. Sansen, *Low-Noise Wide-Band Amplifiers in Bipolar and CMOS Technology*, 1991 Kluwer Academic Publisher, pp. 163 ss.
- [5] K. Larker, W. Sansen, *Design of Analog Integrated Circuit and Systems*, 1994 McGraw-Hill, pp. 31.
- [6] P.O'Connor, G. De Geronimo, "Prospects for charge sensitive amplifiers in scaled CMOS," *Nucl. Sci. Symp. Conference Record*, IEEE, 1999, pp. 89-93 vol. 1.
- [7] G. Gramegna, P. O'Connor, P. Rehak, S. Hart, "CMOS preamplifier for low-capacitance detectors," *Nucl. Inst. Meth.*, A 390 (1997) pp. 241-250.
- [8] B. Krieger, I. Kipnis and B. Ludewigt, "XPS: A multi-channel preamplifier-shaper IC for X-ray spectroscopy," *IEEE Trans. Nucl. Sci.*, vol. 45, pp. 732–734, 1998.
- [9] F. Krummenacher, N. Joehl, "A 4-Mhz continuous-time filter with on chip automatic tuning," *IEEE J. Solid-State Circuits*, vol. 23, pp.750-758, June 1988.
- [10] W. Moses, E. Beuville, and M. Ho, "A Winner-Take-All IC for determining the crystal of interaction in PET detectors," *IEEE Trans. Nucl. Sci.*, vol. 43, pp. 1615-1618, 1996.
- [11] J. Shieh, M. Patil, B. Sheu, "Measurement and analysis of charge injection in MOS analog switches," *IEEE J. Solid-State Circuits*, vol. 22, no.2, April 1987 pp. 277-281.
- [12] D. Su, M. Loinaz, S. Masui, B. Wooley, "Experimental results and modeling techniques for substrate noise in mixed-signal ICs," *IEEE J. Solid-State Circuits*, vol. 28, no.4, April 1993, pp. 426.
- [13] V. Radeka, "Signal, noise and resolution in position-sensitive detectors," *IEEE Trans. Nucl. Sci.*, vol 21, 1974, pp. 51
- [14] G. Gruber, W. Choong, W. Moses, S. Derenzo, S. Holland, M. Pedrali-Noy et al., "Performance of a compact 64-Pixel CsI(Tl)/Si PIN photodiode imaging module with IC readout," *IEEE Trans. Nucl. Sci.*, (Submitted for Publication).